

Spin transport through a quantum network: Effects of Rashba spin orbit interaction and Aharonov-Bohm flux

Moumita Dey[†], Santanu K. Maiti^{†,‡,*}, and S. N. Karmakar[†]

[†]*Theoretical Condensed Matter Physics Division,*

Saha Institute of Nuclear Physics, 1/AF, Bidhannagar, Kolkata-700 064, India

[‡]*Department of Physics, Narasinha Dutt College, 129 Belilious Road, Howrah-711 101, India*

We address spin dependent transport through an array of diamonds in the presence of Rashba spin orbit (SO) interaction where each diamond plaquette is penetrated by an Aharonov-Bohm (AB) flux ϕ . The diamond chain is attached symmetrically to two semi-infinite one-dimensional non-magnetic metallic leads. We adopt a single particle tight-binding Hamiltonian to describe the system and obtain all the results by using Green's function formalism. Following an analytical description of energy dispersion relation of an infinite diamond chain in the presence of Rashba SO interaction, we study numerically the conductance-energy characteristics together with the density of states of a finite sized diamond network to establish the idea. At the typical flux $\phi = \phi_0/2$, a delocalizing effect is observed in the presence of Rashba SO interaction and depending on the specific choices of SO interaction strength and AB flux the quantum network can be used as a spin filter. Our analysis may be inspiring in designing spintronic devices.

PACS numbers: 73.23.-b, 72.25.-b

I. INTRODUCTION

In recent times spin transport in low dimensional systems has drawn much attention from theoretical as well as experimental point of view, due to its promising applications in the field of 'spintronics' [1]. It is a newly developed sub-discipline in condensed matter physics, that deals with the idea of manipulating electron spin in transport phenomena in addition to their charge and holds future promises to integrate memory and logic into a single device. Since the discovery of Giant Magnetoresistance (GMR) effect [2] in Fe-Cr magnetic multilayers revolutionary advancement has taken place in data processing, device making and quantum computation techniques. Today generation of pure spin current is a major challenge to us for further development in quantum computation. A more or less usual way of realization [3, 4] of spin filters is by using ferromagnetic leads or by external magnetic field. But in the first case, spin injection from ferromagnetic leads is difficult due to large resistivity mismatch and for the second one the difficulty is to confine a very strong magnetic field into a small region like a quantum dot (QD). Therefore, attention is being paid for modelling of spin filters using the intrinsic properties [5–10] of mesoscopic systems such as spin orbit interaction or voltage bias. Studies on Rashba spin orbit interaction [11–14], which is present in asymmetric heterostructures has made a significant impact in semiconductor spintronics as far as the control of spin dynamics is concerned. It is generally important in narrow gap semiconductors and its strength can be tuned by electrostatic means i.e., external gate voltages [15–17]. Rashba

SO interaction induces spin flipping through a mechanism known as D'yakonov-Perel' [18] mechanism, which is a slow spin dephasing process in which spin precession takes place around the Rashba field during transmission.

Over the last few years quantum networks are becoming prospective candidates for studying transport phenomena because of the manifestation of several interesting features like, quantum interference effect, interplay of AB flux and network geometry on electron localization, interaction induced delocalization, effect of disorder, electron-electron interaction, etc. It may be interesting to study the effects of Rashba SO coupling and AB flux in such quantum networks. Depending on their topology these geometries exhibit various striking spectral properties and the interplay between AB flux and Rashba SO strength can also be explored. In 2005, Bercioux *et al.* [19] considered the effect of AB flux and Rashba SO interaction on energy averaged conductances for a finite sized diamond chain. They observed that in such a network spin orbit interaction or AB flux can induce complete localization, while the presence of both of them can lead to the effect of weak anti-localization. The possibility to use such a diamond network as a spin filter was explored by Aharony *et al.* in 2008 [20]. In 2009, there was another work by Chakrabarti *et al.* [21], where they have shown how such a diamond network can be implemented as a p-type or n-type semiconductor depending on the suitable choice of the on site potentials of the atoms at the vertices of the network and the strength of the magnetic flux penetrating each diamond plaquette. But the effect of spin orbit interaction was not considered. In our present work, we wish to explore various spectral features in presence of both AB flux and Rashba SO interaction. We calculate spin conserved and spin flip conductances using single particle Green's function formalism [22] within a tight-binding framework for a finite sized diamond chain, which is in agreement with the an-

*Corresponding Author: Santanu K. Maiti
Electronic mail: santanu.maiti@saha.ac.in

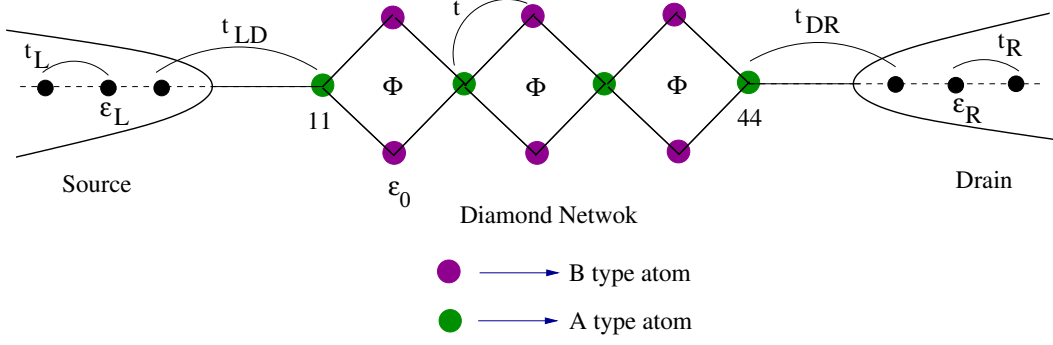


FIG. 1: (Color online). A finite sized diamond network (central region) connected to two semi-infinite one-dimensional non-magnetic metallic leads, viz, source and drain. The diamond network is composed of two types of atoms labelled by filled green and blue circles, where each diamond plaquette is penetrated by an AB flux ϕ .

alytical dispersion relation obtained for an infinite diamond network. We also observe the variation of density of states (DOS) and the effect of Rashba SO interaction on electron localization. Finally, we show that, for some specific choices of external parameters this finite sized diamond network can achieve a high degree of spin polarization.

Our organization of the paper is as follows. Following a brief introduction (Section I), in Section II, we present the model and the theoretical formulation. Section III explores the significant results which contain an analytical description of the energy dispersion relation for an infinite diamond network and the numerical calculations of two-terminal conductance, DOS, delocalizing effect in presence of SO interaction and spin filtering action for a finite sized diamond array. At the end, the summary of our work will be available in Section IV.

II. MODEL AND SYNOPSIS OF THE THEORETICAL FORMULATION

At the beginning of our theoretical formulation we start by describing the geometry of the quasi one-dimensional nanostructure through which spin transport properties are being investigated. In Fig. 1 we illustrate schematically the quantum network, in which the square loops are connected at the vertices (termed as Diamond Network (DN) or Diamond Chain (DC)). The diamond array is connected symmetrically to two semi-infinite one-dimensional (1D) non-magnetic metallic leads commonly known as source and drain those are characterized by the electrochemical potentials μ_1 and μ_2 under the non-equilibrium condition when a bias voltage is applied.

The full Hamiltonian for the complete system i.e., source-DN-drain can be written as,

$$H = H_D + H_L + H_R + H_{LD} + H_{DR} \quad (1)$$

where, H_D represents the Hamiltonian for the diamond network. $H_{L(R)}$ corresponds to the Hamiltonian for the

left (right) lead, i.e., source (drain), and $H_{LD(DR)}$ is the Hamiltonian describing the chain-lead coupling.

The Hamiltonian for the diamond network can be written in a single electron picture within the framework of tight-binding formulation in Wannier basis, using nearest-neighbor approximation as,

$$\begin{aligned} H_D = & \sum_{l,m} c_{l,m}^\dagger \epsilon_0 c_{l,m} + \sum_{l,m} \left(c_{l,m}^\dagger \mathbf{t} e^{i\alpha} c_{l+1,m} + \text{h.c.} \right) \\ & + \sum_{l,m} \left(c_{l,m}^\dagger \mathbf{t} e^{i\alpha} c_{l,m+1} + \text{h.c.} \right) \\ & + \sum_{l,m} \left(c_{l,m}^\dagger (i\sigma_y) \mathbf{tso} e^{i\alpha} c_{l+1,m} + \text{h.c.} \right) \\ & + \sum_{l,m} \left(c_{l,m}^\dagger (i\sigma_x) \mathbf{tso} e^{i\alpha} c_{l,m+1} + \text{h.c.} \right) \quad (2) \end{aligned}$$

where,

$$\begin{aligned} \mathbf{c}_{l,m}^\dagger &= \begin{pmatrix} c_{l,m\uparrow}^\dagger & c_{l,m\downarrow}^\dagger \end{pmatrix}; \quad \mathbf{c}_{l,m} = \begin{pmatrix} c_{l,m\uparrow} \\ c_{l,m\downarrow} \end{pmatrix}; \\ \epsilon_0 &= \begin{pmatrix} \epsilon_0 & 0 \\ 0 & \epsilon_0 \end{pmatrix}; \quad \mathbf{t} = t \begin{pmatrix} 1 & 0 \\ 0 & 1 \end{pmatrix}; \quad \mathbf{tso} = \begin{pmatrix} tso & 0 \\ 0 & tso \end{pmatrix} \end{aligned}$$

First term of Eq. (2) represents the effective on-site energies of the atomic sites in the network. ϵ_0 being the magnitude of the site energy associated with each atomic site of the diamond chain. For A type of atoms $\epsilon_0 = \epsilon_A$, while for B type of atoms we call ϵ_0 as ϵ_B . The second and third terms represent the electron hopping along X and Y directions, respectively, where t is the nearest-neighbor hopping strength and $\alpha = \frac{2\pi\phi}{4\phi_0}$ is the phase factor due to the flux ϕ threaded by each diamond plaquette. Here we use double indexing to describe the location of lattice sites in the diamond network, and for our illustrative purpose in Fig. 2 we describe it schematically for a single plaquette. The fourth and fifth terms are associated with the spin dependent Rashba interaction, where tso is the isotropic nearest-neighbor transfer integral that measures the strength of Rashba SO coupling.

Similarly, the Hamiltonian $H_{L(R)}$ for the two leads can

be written as,

$$H_{L(R)} = \sum_i \mathbf{c}_i^\dagger \epsilon_{L(R)} \mathbf{c}_i + \sum_i \left(\mathbf{c}_i^\dagger t_{L(R)} \mathbf{c}_{i+1} + \text{h.c.} \right) \quad (3)$$

where, $\epsilon_{L(R)}$'s are the site energies and $t_{L(R)}$ is the hopping strength between the nearest-neighbor sites of the leads.

Here also,

$$\epsilon_{L(R)} = \begin{pmatrix} \epsilon_{L(R)} & 0 \\ 0 & \epsilon_{L(R)} \end{pmatrix}; \quad \mathbf{t}_{L(R)} = \begin{pmatrix} t_{L(R)} & 0 \\ 0 & t_{L(R)} \end{pmatrix}$$

The diamond chain-to-lead coupling Hamiltonian is described by,

$$H_{LD(DR)} = \left(\mathbf{c}_{0(NN)}^\dagger \mathbf{t}_{LD(DR)} \mathbf{c}_{1(N+1)} + \text{h.c.} \right) \quad (4)$$

where, $t_{LD(DR)}$ being the chain-lead coupling strength.

In order to calculate spin dependent transmission probabilities through the quantum network, we use single particle Green's function formalism. Within the regime of

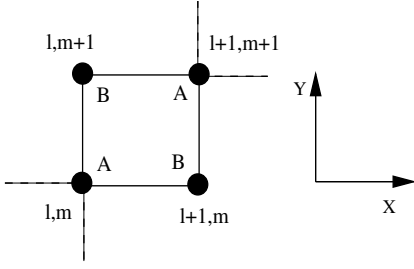


FIG. 2: (Color online). Index convention for representing the co-ordinates. l and m denote the co-ordinates along the X and Y directions, respectively.

coherent transport and in absence of Coulomb interaction this technique is well applied.

The single particle Green's function representing the full system for an electron with energy E is defined as,

$$\mathbf{G} = (\mathbf{E} - \mathbf{H})^{-1} \quad (5)$$

where,

$$\mathbf{E} = (\epsilon + i\eta)\mathbf{I} \quad (6)$$

In the above expression $i\eta$ is a small imaginary term added to the energy ϵ to make the Green's function \mathbf{G} non-hermitian.

Now, \mathbf{H} and \mathbf{G} representing the Hamiltonian and the Green's function for the full system those can be partitioned in terms of different sub-Hamiltonians like,

$$\mathbf{H} = \begin{pmatrix} \mathbf{H}_L & \mathbf{H}_{LD} & 0 \\ \mathbf{H}_{LD}^\dagger & \mathbf{H}_D & \mathbf{H}_{DR} \\ 0 & \mathbf{H}_{DR}^\dagger & \mathbf{H}_R \end{pmatrix} \quad (7)$$

$$\mathbf{G} = \begin{pmatrix} \mathbf{G}_L & \mathbf{G}_{LD} & 0 \\ \mathbf{G}_{LD}^\dagger & \mathbf{G}_D & \mathbf{G}_{DR} \\ 0 & \mathbf{G}_{DR}^\dagger & \mathbf{G}_R \end{pmatrix} \quad (8)$$

where, \mathbf{H}_L , \mathbf{H}_D and \mathbf{H}_R represent the Hamiltonians (in matrix form) for the left lead, diamond network and right lead, respectively. \mathbf{H}_{LD} and \mathbf{H}_{DR} are the matrices for the Hamiltonians representing the diamond network-lead coupling. Assuming that there is no direct coupling between the leads themselves, the corner elements of the matrices are zero. A similar definition goes for the Green's function matrix \mathbf{G} as well.

Our first goal is to determine \mathbf{G}_D (Green's function for the network only) which defines all physical quantities of interest. Following Eq. (5) and using the block matrix form of \mathbf{H} and \mathbf{G} the form of \mathbf{G}_D can be expressed as,

$$\mathbf{G}_D = (\mathbf{E} - \mathbf{H}_D - \Sigma_L - \Sigma_R)^{-1} \quad (9)$$

where, Σ_L and Σ_R represent the contact self-energies introduced to incorporate the effects of semi-infinite leads coupled to the system, and, they are expressed by the relations,

$$\begin{aligned} \Sigma_L &= \mathbf{H}_{LD}^\dagger \mathbf{G}_D \mathbf{H}_{LD} \\ \Sigma_R &= \mathbf{H}_{DR}^\dagger \mathbf{G}_D \mathbf{H}_{DR} \end{aligned} \quad (10)$$

Thus, the form of self-energies are independent of the nano-structure itself through which transmission is studied and they completely describe the influence of two leads attached to the system. Now, the transmission probability ($T_{\sigma\sigma'}$) of an electron with energy E is related to the Green's function as,

$$\begin{aligned} T_{\sigma\sigma'} &= \Gamma_{L(\sigma\sigma)}^1 \mathbf{G}_{r(\sigma\sigma')}^{1N} \mathbf{G}_{a(\sigma'\sigma)}^{N1} \Gamma_{R(\sigma'\sigma')}^N \\ &= \Gamma_{L(\sigma\sigma)}^1 |\mathbf{G}_{(\sigma\sigma')}^{1N}|^2 \Gamma_{R(\sigma'\sigma')}^N \end{aligned} \quad (11)$$

where, $\Gamma_{L(\sigma\sigma)}^1 = \langle 11\sigma | \Gamma_L | 11\sigma \rangle$, $\Gamma_{R(\sigma'\sigma')}^N = \langle NN\sigma' | \Gamma_R | NN\sigma' \rangle$ and $\mathbf{G}_{\sigma\sigma'}^{1N} = \langle 11\sigma | \mathbf{G} | NN\sigma' \rangle$. Here, \mathbf{G}_r and \mathbf{G}_a are the retarded and advanced single particle Green's functions (for the network only) for an electron with energy E . Γ_L and Γ_R are the coupling matrices, representing the coupling of the quantum network to left and right leads, respectively, and they are defined by the relation,

$$\Gamma_{L(R)} = i \left[\Sigma_{L(R)}^r - \Sigma_{L(R)}^a \right] \quad (12)$$

Here, $\Sigma_{L(R)}^r$ and $\Sigma_{L(R)}^a$ are the retarded and advanced self-energies, respectively, and they are conjugate to each other. It is shown in literature by Datta *et al.* [22] that the self-energy can be expressed as a linear combination of a real and an imaginary part in the form,

$$\Sigma_{L(R)}^r = \Lambda_{L(R)} - i\Delta_{L(R)} \quad (13)$$

The real part of self-energy describes the shift of the energy levels and the imaginary part corresponds to the broadening of the levels. The finite imaginary part appears due to incorporation of the semi-infinite leads having continuous energy spectrum. Therefore, the coupling

matrices can easily be obtained from the self-energy expression and is expressed as,

$$\mathbf{\Gamma}_{L(R)} = -2\text{Im}(\mathbf{\Sigma}_{L(R)}) \quad (14)$$

Considering linear transport regime, conductance (g_σ) is obtained using two-terminal Landauer conductance formula,

$$g_{\sigma\sigma'} = \frac{e^2}{h} T_{\sigma\sigma'} \quad (15)$$

Throughout our study we choose $c = e = h = 1$ to simplify the unit system.

III. NUMERICAL RESULTS AND DISCUSSION

In this section we study spin dependent transport through a diamond chain in presence of Rashba spin orbit interaction and magnetic flux and the interplay between them. An array of diamonds is a bipartite structure with lattice sites having different co-ordination numbers. Electron localization plays a significant role even in the absence of disorder in this kind of geometry due to quantum interference effect. First we obtain analytically the dispersion relation for an infinite diamond chain in the presence of magnetic flux and Rashba interaction. Next, we simulate numerically various features of spin transport using a finite size diamond chain. Now, before analyzing the results we mention all the parameters those are used for numerical simulations. Our first assumption is that the two non-magnetic side-attached leads are made up of identical materials. The on-site energies in the two leads ($\epsilon_{L(R)}$) are set as 0. Hopping strength between the sites in the leads is chosen as $t_{L(R)} = 4$, whereas in the diamond chain it is set as $t = 3$. The Rashba strength (tso) is chosen to be uniform along X and Y directions and throughout the calculation its magnitude is considered as comparable to t . Energy scale is fixed in unit of t . Throughout the analysis we present all the results considering the chain-to-electrode coupling strength as $t_{LD} = t_{DR} = 2.5$

A. Energy dispersion relation in presence of Rashba SO interaction and magnetic flux

The energy dispersion relation for an infinite diamond chain clearly depicts several significant features of this kind of topology. In order to study the E - k relation theoretically first we map the quasi one-dimensional diamond network into a linear chain with modified site energy and hopping strength.

We start with the general difference equation for an arbitrary site (n, p) , where n and p denote the indexing along X and Y directions, respectively, as

$$(\mathbf{E} - \epsilon)\psi_{\mathbf{n}\mathbf{p}} = \mathbf{t}_{\mathbf{x}_+}\psi_{\mathbf{n}+1,\mathbf{p}} + \mathbf{t}_{\mathbf{x}_-}\psi_{\mathbf{n}-1,\mathbf{p}} + \mathbf{t}_{\mathbf{y}_+}\psi_{\mathbf{n},\mathbf{p}+1} + \mathbf{t}_{\mathbf{y}_-}\psi_{\mathbf{n},\mathbf{p}-1} \quad (16)$$

where,

$$\mathbf{t}_{\mathbf{x}_+} = \begin{pmatrix} te^{\mp i\alpha} & tso \\ -tso & te^{\mp i\alpha} \end{pmatrix}$$

$$\mathbf{t}_{\mathbf{x}_-} = \begin{pmatrix} te^{\pm i\alpha} & -tso \\ tso & te^{\pm i\alpha} \end{pmatrix}$$

$$\mathbf{t}_{\mathbf{y}_+} = \begin{pmatrix} te^{\pm i\alpha} & itso \\ itso & te^{\pm i\alpha} \end{pmatrix}$$

$$\mathbf{t}_{\mathbf{y}_-} = \begin{pmatrix} te^{\mp i\alpha} & -itso \\ -itso & te^{\mp i\alpha} \end{pmatrix}$$

$$\mathbf{E} = \begin{pmatrix} E & 0 \\ 0 & E \end{pmatrix}; \epsilon = \begin{pmatrix} \epsilon_0 & 0 \\ 0 & \epsilon_0 \end{pmatrix}; \text{ and } \psi_{\mathbf{n}\mathbf{p}} = \begin{pmatrix} \psi_{np,\uparrow} \\ \psi_{np,\downarrow} \end{pmatrix}$$

ϕ being the AB flux enclosed by each diamond plaquette and $\phi_0 = ch/e$, the elementary flux-quantum.

We begin the decimation technique by writing down the difference equations at the sites containing A and B type atoms (see Fig. 2). The equations are given below.

$$\begin{aligned} (\mathbf{E} - \epsilon_{\mathbf{B}})\psi_{12} &= e^{i\alpha}\mathbf{t}_{\mathbf{x}_+}\psi_{22} + e^{-i\alpha}\mathbf{t}_{\mathbf{y}_-}\psi_{11} \\ (\mathbf{E} - \epsilon_{\mathbf{B}})\psi_{21} &= e^{i\alpha}\mathbf{t}_{\mathbf{x}_-}\psi_{11} + e^{-i\alpha}\mathbf{t}_{\mathbf{y}_+}\psi_{22} \\ (\mathbf{E} - \epsilon_{\mathbf{B}})\psi_{23} &= e^{i\alpha}\mathbf{t}_{\mathbf{x}_+}\psi_{33} + e^{-i\alpha}\mathbf{t}_{\mathbf{y}_-}\psi_{22} \\ (\mathbf{E} - \epsilon_{\mathbf{B}})\psi_{23} &= e^{i\alpha}\mathbf{t}_{\mathbf{x}_-}\psi_{22} + e^{-i\alpha}\mathbf{t}_{\mathbf{y}_+}\psi_{33} \end{aligned} \quad (17)$$

and,

$$\begin{aligned} (\mathbf{E} - \epsilon_{\mathbf{A}})\psi_{22} &= e^{-i\alpha}\mathbf{t}_{\mathbf{x}_+}\psi_{32} + e^{-i\alpha}\mathbf{t}_{\mathbf{x}_-}\psi_{12} \\ &+ e^{i\alpha}\mathbf{t}_{\mathbf{y}_+}\psi_{23} + e^{i\alpha}\mathbf{t}_{\mathbf{y}_-}\psi_{33} \end{aligned} \quad (18)$$

Substituting ψ_{32} , ψ_{12} , ψ_{23} and ψ_{33} from Eq. (17) in Eq. (18) we get,

$$(\mathbf{E} - \epsilon')\psi_{22} = \mathbf{t}_{\mathbf{b}}\psi_{11} + \mathbf{t}_{\mathbf{f}}\psi_{33} \quad (19)$$

This represents the difference equation for an infinite linear chain with modified site energy ϵ' and the forward and backward hopping strengths $\mathbf{t}_{\mathbf{f}}$ and $\mathbf{t}_{\mathbf{b}}$, respectively. These quantities are expressed as follows.

$$\begin{aligned} \epsilon' &= \epsilon_{\mathbf{A}} + \mathbf{t}_{\mathbf{x}_+} \cdot (\mathbf{E} - \epsilon_{\mathbf{B}})^{-1} \cdot \mathbf{t}_{\mathbf{x}_-} + \mathbf{t}_{\mathbf{x}_-} \cdot (\mathbf{E} - \epsilon_{\mathbf{B}})^{-1} \cdot \mathbf{t}_{\mathbf{x}_+} \\ &+ \mathbf{t}_{\mathbf{y}_+} \cdot (\mathbf{E} - \epsilon_{\mathbf{B}})^{-1} \cdot \mathbf{t}_{\mathbf{y}_-} + \mathbf{t}_{\mathbf{y}_-} \cdot (\mathbf{E} - \epsilon_{\mathbf{B}})^{-1} \cdot \mathbf{t}_{\mathbf{y}_+} \\ \mathbf{t}_{\mathbf{b}} &= e^{-2i\alpha}\mathbf{t}_{\mathbf{x}_-} \cdot (\mathbf{E} - \epsilon_{\mathbf{B}})^{-1} \cdot \mathbf{t}_{\mathbf{y}_-} + e^{2i\alpha}\mathbf{t}_{\mathbf{y}_-} \cdot (\mathbf{E} - \epsilon_{\mathbf{B}})^{-1} \cdot \mathbf{t}_{\mathbf{x}_-} \\ \mathbf{t}_{\mathbf{f}} &= e^{-2i\alpha}\mathbf{t}_{\mathbf{x}_+} \cdot (\mathbf{E} - \epsilon_{\mathbf{B}})^{-1} \cdot \mathbf{t}_{\mathbf{y}_+} + e^{2i\alpha}\mathbf{t}_{\mathbf{y}_+} \cdot (\mathbf{E} - \epsilon_{\mathbf{B}})^{-1} \cdot \mathbf{t}_{\mathbf{x}_+} \end{aligned} \quad (20)$$

As the translational invariance is preserved in this decimated infinite linear chain the solution will have Bloch form and it can be written as,

$$\psi_{\mathbf{n}} = \sum_k e^{ikna} \begin{pmatrix} \psi_{k,\uparrow} \\ \psi_{k,\downarrow} \end{pmatrix} \quad (21)$$

ψ_n being a short form of ψ_{nn} .

Using this form of ψ_n , the difference equation for an arbitrary site n can be expressed as,

$$\sum_k (E - \epsilon') \begin{pmatrix} \psi_{k,\uparrow} \\ \psi_{k,\downarrow} \end{pmatrix} e^{ikna} = t_f \sum_k \begin{pmatrix} \psi_{k,\uparrow} \\ \psi_{k,\downarrow} \end{pmatrix} e^{ik(n+1)a}$$

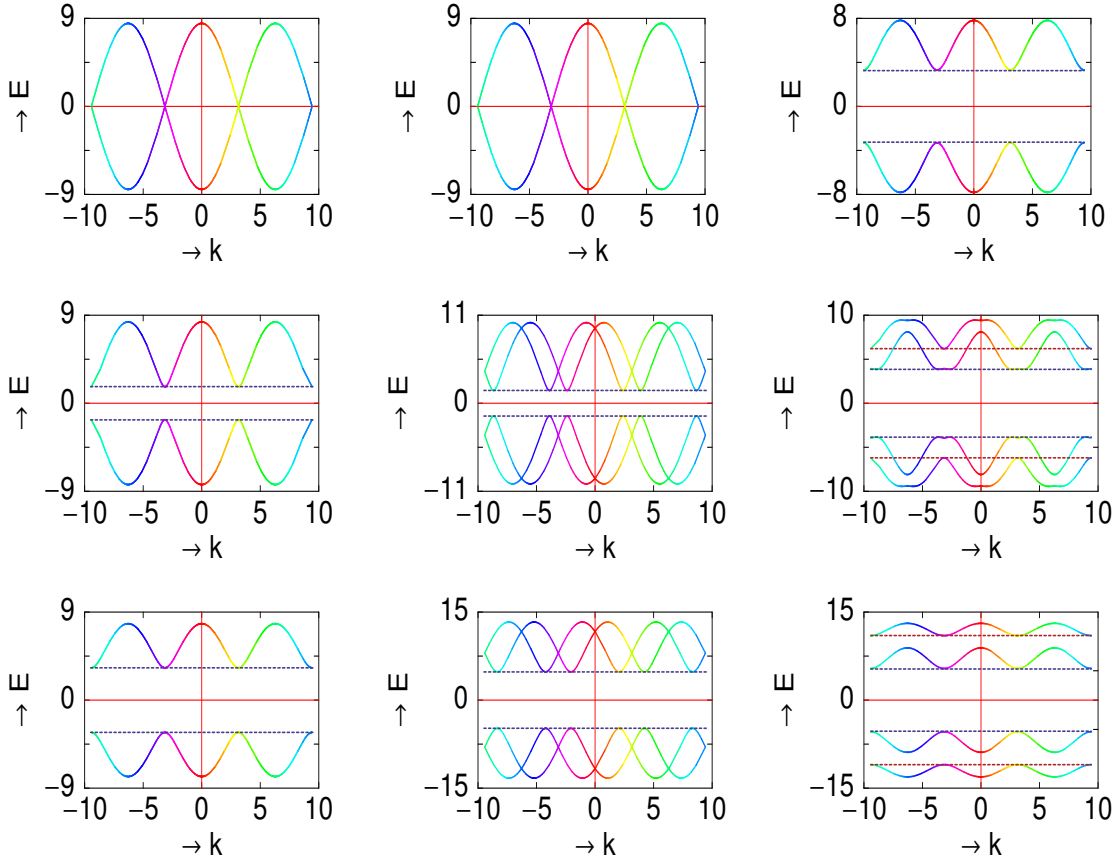


FIG. 3: (Color online). Energy dispersion (E - k) curves for an infinite diamond chain with $\epsilon_A = \epsilon_B = 0$. The upper, middle and lower spectra in the 1st column correspond to $\phi = 0, 0.2$ and 0.4 , respectively, when $tso = 0$. In the 2nd column three different spectra from the top represent the results for $tso = 0, 2$ and 4 , respectively, when ϕ is set to 0 . Finally, the three different figures in the last column refer to the results for the identical values of tso considered in the 2nd column when ϕ is fixed at 0.4 .

$$+ t_b \sum_k \begin{pmatrix} \psi_{k,\uparrow} \\ \psi_{k,\downarrow} \end{pmatrix} e^{ik(n-1)a} \quad (22)$$

For the non-trivial solution of Eq. (22) we have the relation,

$$\mathbf{Det}[\mathbf{M}] = 0 \quad (23)$$

where, $\mathbf{M} = (\mathbf{E} - \epsilon - \mathbf{t}_f e^{ika} - \mathbf{t}_b e^{-ika})$.

Expanding Eq. (23) we obtain a 4-th degree polynomial of E and simplifying it we get the E - k relation in terms of the parameters ϕ and tso . E corresponds to energy of the states which is a linear combination of up ($k \uparrow$) and down ($k \downarrow$) states.

Following the above mathematical treatment, in Fig. 3 we show the variation of energy E as a function k for some typical parameter values of ϕ and tso . The first column corresponds to the results for some specific values of AB flux ϕ in the absence of Rashba SO coupling i.e., $tso = 0$. It is observed that for zero magnetic flux the spectrum is degenerate and gapless, whereas a small non-zero flux

($\phi = 0.2$) opens a gap symmetrically around $E = 0$ preserving the degeneracy. Here we choose $\epsilon_A = \epsilon_B = 0$ and the gap appears symmetrically as long as ϕ is introduced, but the point is that for unequal values of ϵ_A and ϵ_B gap always appears even in the absence of ϕ (which is not shown in the figure). The width of the gap increases symmetrically with the rise in ϕ . In the second column of Fig. 3 we show the energy dispersion curves for the three different values of Rashba SO coupling strength keeping $\phi = 0$, where the upper, middle and lower spectra correspond to $tso = 0, 2$ and 4 , respectively. The upper spectrum is gapless and degenerate as described earlier. For non-zero values of tso , the energy spectrum gets splitted vertically and all the degeneracies are removed except at the points $k = n\pi$, where $n = 0, \pm 1, \pm 2, \dots$. The gap becomes widened with the increase in Rashba strength as clearly noticed from the middle and lower spectra. The above features seem to be more interesting when a non-zero magnetic flux is applied. In this case, each subband gets separated vertically as illustrated in the third column of Fig. 3. With a sufficiently high magnetic flux

($\phi = 0.4$) and Rashba strength ($tso = 4$) two additional gaps occur in the dispersion spectrum along with the previous one, and these gaps can be *controlled externally by tuning the AB flux or the Rashba strength*. It provides an important signature in designing nano-scale spintronic devices.

B. Variation of conductances with AB flux

In Fig. 4 we plot conductance-flux characteristics for a diamond network both in the presence and absence of Rashba SO interaction. The results are computed at the typical energy $E = 5$ considering five diamond plaquettes, where the green and red curves correspond to $tso = 0$ and 2, respectively. It is observed that in the ab-

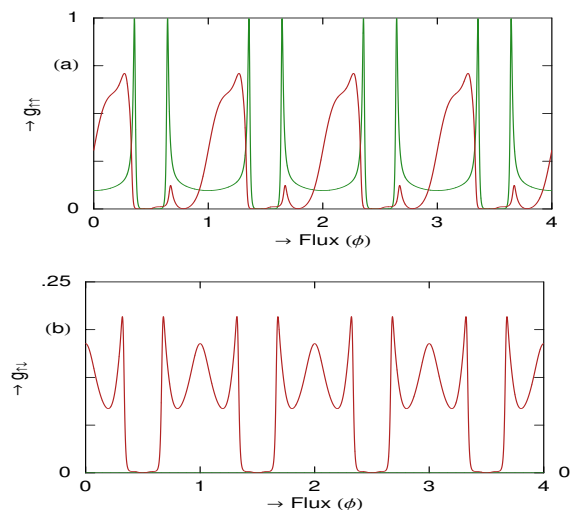


FIG. 4: (Color online). Variations of $g_{\uparrow\uparrow}$ (a) and $g_{\uparrow\downarrow}$ (b) with AB flux ϕ for a diamond chain considering 5 plaquettes at the typical energy $E = 5$. The green and red curves correspond to $tso = 0$ and 2, respectively. Here we set $\epsilon_A = \epsilon_B = 0$.

sence of Rashba coupling spin flip conductance $g_{\uparrow\downarrow}$ drops exactly to zero for the entire range of ϕ (green curve of Fig. 4(b)), while spin conserved conductance $g_{\uparrow\uparrow}$ persists and it provides ϕ_0 flux-quantum periodicity as a function of ϕ . Interestingly we see that $g_{\uparrow\uparrow}$ completely vanishes at the typical flux $\phi = \phi_0/2$ (see green curve of Fig. 4(a)) due to the complete destructive interference among the electronic waves passing through different arms of the plaquettes. On the other hand, in presence of Rashba SO interaction both $g_{\uparrow\uparrow}$ and $g_{\uparrow\downarrow}$ show finite value for wide ranges of ϕ and a significant change in their amplitudes takes place compared to the case where $tso = 0$. In presence of the SO interaction, the oscillatory character of the conductances is still preserved providing traditional ϕ_0 flux-quantum periodicity. The important feature is that for non-zero value of tso , spin flip conductance disappears at the typical flux $\phi = \phi_0/2$. Since $g_{\downarrow\downarrow}$ and $g_{\downarrow\uparrow}$ show exactly identical behavior to those mentioned for

$g_{\uparrow\uparrow}$ and $g_{\uparrow\downarrow}$, respectively, we do not display these results further.

The above numerical features can be justified from the following analytical treatment.

To illustrate the different features of AB oscillation both in presence and absence of Rashba SO interaction, we consider an ideal 1D square loop threaded by an AB flux ϕ , as shown schematically in Fig. 5. Two semi-infinite one-dimensional leads are to be connected at the vertices A and B of the square loop. Rashba SO inter-

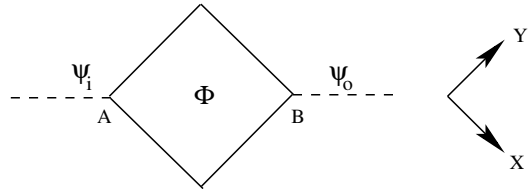


FIG. 5: (Color online). A single diamond plaquette threaded by an AB flux ϕ . ψ_i and ψ_o denote the incoming and outgoing waves, respectively.

action is considered to be present only in the loop and not in the leads. If ψ_i and ψ_o describe the incoming and outgoing wave functions at the respective points A and B, then ψ_o can be obtained considering only 1st order tunneling processes as,

$$\psi_o = \frac{1}{2} \left(e^{-i\frac{\gamma}{2} \mathbf{R}_x(\theta) \mathbf{R}_y(\theta)} + e^{i\frac{\gamma}{2} \mathbf{R}_y(\theta) \mathbf{R}_x(\theta)} \right) \psi_i \quad (24)$$

where, $\gamma = \frac{2\pi\phi}{\phi_0}$. $\mathbf{R}_\hat{r}(\theta)$ is the rotation operator defined by the relation,

$$\mathbf{R}_\hat{r}(\theta) = \mathbf{I} \cos \frac{\theta}{2} - i\hat{r} \cdot \vec{\sigma} \sin \frac{\theta}{2} \quad (25)$$

where, $\theta = \frac{2m^* \alpha_R L}{\hbar^2}$ is the spin precession angle. α_R is the strength of Rashba SO interaction and L represents the length of each side of the square loop. The wave functions ψ_i and ψ_o used in Eq. (24) are defined as follows.

$$\psi_o = \begin{pmatrix} \psi_{o,\uparrow} \\ \psi_{o,\downarrow} \end{pmatrix} \text{ and } \psi_i = \begin{pmatrix} \psi_{i,\uparrow} \\ \psi_{i,\downarrow} \end{pmatrix}$$

Following Eq. (25) the matrices $\mathbf{R}_x(\theta)$ and $\mathbf{R}_y(\theta)$ can be written as given below.

$$\mathbf{R}_x(\theta) = \begin{pmatrix} \cos \frac{\theta}{2} & -i \sin \frac{\theta}{2} \\ -i \sin \frac{\theta}{2} & \cos \frac{\theta}{2} \end{pmatrix}$$

$$\mathbf{R}_y(\theta) = \begin{pmatrix} \cos \frac{\theta}{2} & -\sin \frac{\theta}{2} \\ \sin \frac{\theta}{2} & \cos \frac{\theta}{2} \end{pmatrix}$$

With these matrix forms we can express the wave functions $\psi_{o,\uparrow}$ and $\psi_{o,\downarrow}$ as linear combinations of $\psi_{i,\uparrow}$ and $\psi_{i,\downarrow}$ by expanding Eq. (24) as,

$$\begin{aligned} |\psi_{o,\uparrow}\rangle &= c_{\uparrow\uparrow} |\psi_{i,\uparrow}\rangle + c_{\downarrow\uparrow} |\psi_{i,\downarrow}\rangle \\ |\psi_{o,\downarrow}\rangle &= c_{\uparrow\downarrow} |\psi_{i,\uparrow}\rangle + c_{\downarrow\downarrow} |\psi_{i,\downarrow}\rangle \end{aligned} \quad (26)$$

where, the co-efficients $c_{\sigma\sigma'}$ are functions of θ and ϕ .

Now the probability of getting an up spin electron at the point B, for the incidence of an electron with up spin at the point A i.e., the spin conserved transmission probability $T_{\uparrow\uparrow}$ is proportional to $|\langle\psi_{i,\uparrow}|\psi_{o,\uparrow}\rangle|^2$, viz, $|c_{\uparrow\uparrow}|^2$. Similarly, the probability of getting a down spin electron with up spin incidence i.e., the spin flip transmission probability $T_{\uparrow\downarrow}$ is proportional to $|\langle\psi_{i,\uparrow}|\psi_{o,\downarrow}\rangle|^2$, viz, $|c_{\uparrow\downarrow}|^2$. After a few mathematical steps the quantities $|c_{\uparrow\uparrow}|^2$ and $|c_{\uparrow\downarrow}|^2$ are expressed as,

$$|c_{\uparrow\uparrow}|^2 = \frac{1}{8}e^{-i\frac{2\pi\phi}{\phi_0}} \left[1 + i\cos\theta + e^{i\frac{2\pi\phi}{\phi_0}}(i + \cos\theta) \right] \times \left[\cos\theta - i + e^{i\frac{2\pi\phi}{\phi_0}}(1 - i\cos\theta) \right] \quad (27)$$

and

$$|c_{\uparrow\downarrow}|^2 = \frac{1}{8}e^{-i\frac{2\pi\phi}{\phi_0}} \left(1 + e^{i\frac{2\pi\phi}{\phi_0}} \right)^2 \sin^2\theta \quad (28)$$

In the absence of Rashba SO interaction $\theta = 0$ since $\alpha_R = 0$, and then the above two equations can be simplified as follows.

$$|c_{\uparrow\uparrow}|^2 = \frac{1}{2} \left[1 + \cos\left(\frac{2\pi\phi}{\phi_0}\right) \right] \quad (29)$$

and

$$|c_{\uparrow\downarrow}|^2 = 0 \quad (30)$$

With the last four mathematical expressions (Eqs. (27)-(30)) we can clearly justify the essential features those are presented in Fig. 4. In the absence of Rashba SO interaction, spin flip conductance vanishes for the entire range of ϕ (see green curve of Fig. 4(b)) following Eq. (30). On the other hand, a oscillatory character of up spin conductance with ϕ_0 periodicity in the absence of tso (green curve of Fig. 4(a)) is followed from Eq. (29). The vanishing behavior of $g_{\uparrow\uparrow}$ at the typical flux $\phi = \phi_0/2$ is also justified from Eq. (29). In the presence of SO interaction, both pure spin transmission and spin flip transmission get modified satisfying Eqs. (27) and (28), respectively. For finite value of tso , spin flip conductance always vanishes at $\phi = \phi_0/2$ obeying Eq. (28).

C. Conductance-energy characteristics

Now we focus our attention on conductance-energy characteristics of a finite sized diamond network for some specific values of AB flux ϕ and Rashba SO interaction strength tso .

In Fig. 6 we plot up spin conductances ($g_{\uparrow\uparrow}$) as a function of injecting electron energy (E) for a diamond network considering 15 identical plaquettes in the absence of Rashba interaction. The top, middle and bottom spectra correspond to AB flux $\phi = 0, 0.2$ and 0.4 , respectively. When $\phi = 0$, the spectrum is gapless (Fig. 6(a)). The

presence of ϕ opens a gap and the width of the gap increases with the rise in ϕ as clearly shown from Figs. 6(b) and (c). This gap is symmetric around the energy $E = 0$ since here we choose $\epsilon_A = \epsilon_B = 0$. On the other hand, if the site energies ϵ_A and ϵ_B are unequal then a gap in the conductance spectrum appears (not shown in the figure) even in the absence of magnetic flux for an infinite chain as well as for a finite sized diamond array. This gap will be symmetric across $E = 0$ provided their (ϵ_A and ϵ_B) magnitudes are identical to each other and the width of the gap increases symmetrically about the center of the gap with the enhancement in ϕ . In this particular case

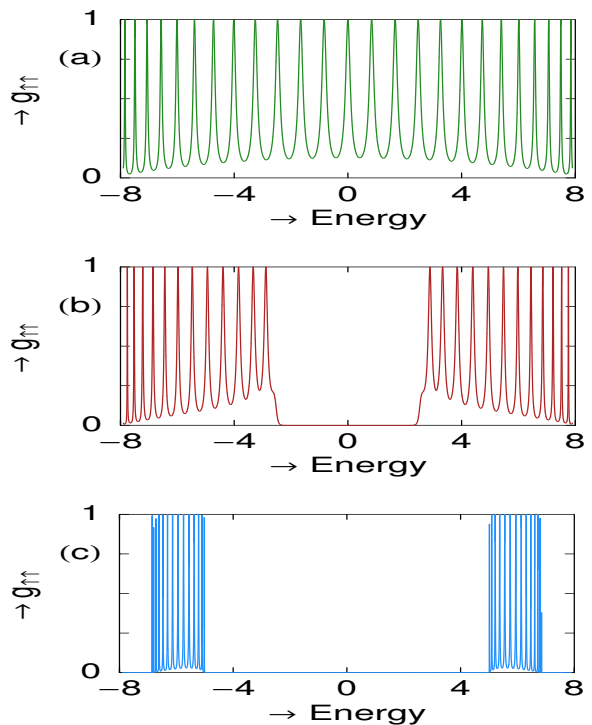


FIG. 6: (Color online). Conductance-energy ($g_{\uparrow\uparrow}$ - E) characteristics in the absence of Rashba SO strength for a diamond network considering 15 diamond plaquettes with $\epsilon_A = \epsilon_B = 0$. (a), (b) and (c) correspond to $\phi = 0, 0.2$ and 0.4 , respectively.

we do not consider any Rashba interaction, and therefore, no spin flip transmission takes place.

In Fig. 7 we show the conductance-energy characteristics of a diamond network with 15 plaquettes in the absence of magnetic flux ϕ for different values of tso . The 1st, 2nd and 3rd rows correspond to the results when $tso = 0, 2$ and 4 , respectively. The spin conserved conductances ($g_{\uparrow\uparrow}$) are plotted in the first column, while in the second column spin flip conductances ($g_{\uparrow\downarrow}$) are given. In absence of tso , gapless spectrum is observed for spin conserved conductance, while spin flip conductance vanishes for the entire energy range. For all other cases, a gap appears in the spectrum and the width of which can be regulated by tuning the Rashba coupling strength.

The most interesting features in the conductance-

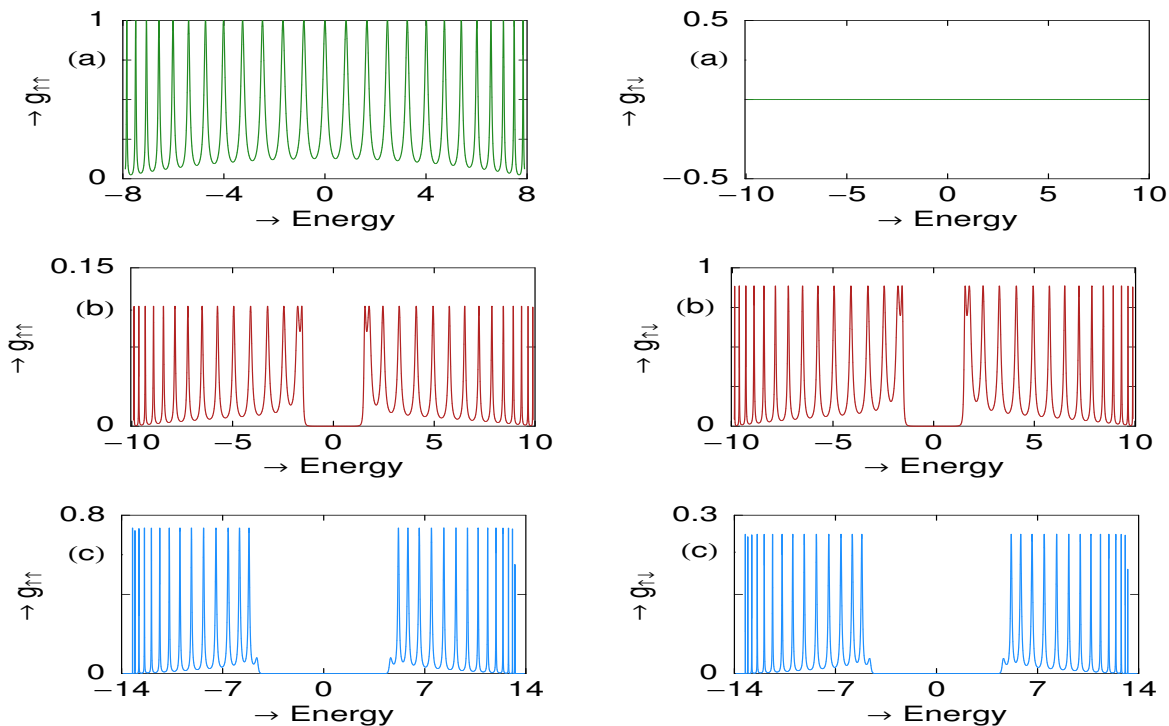


FIG. 7: (Color online). $g_{\uparrow\uparrow}$ and $g_{\uparrow\downarrow}$ as a function of energy E for a diamond chain with 15 plaquettes considering $\epsilon_A = \epsilon_B = 0$ in the absence of AB flux ϕ . The 1st, 2nd and 3rd rows represent the results when $tso = 0, 2$ and 4 , respectively.

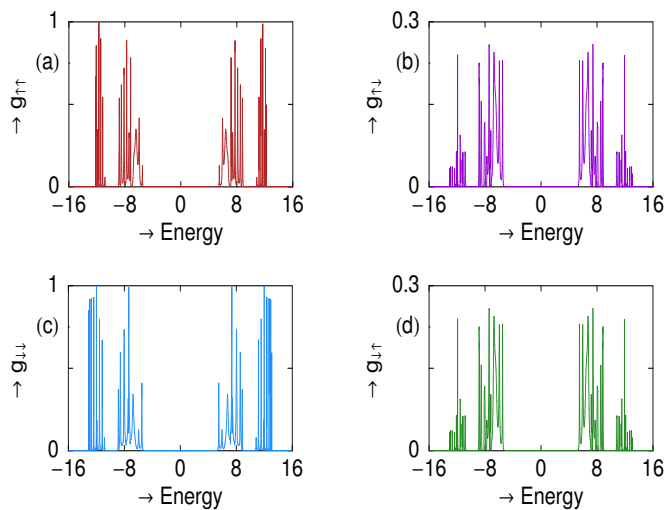


FIG. 8: (Color online). Spin conserved ($g_{\uparrow\uparrow}$, $g_{\downarrow\downarrow}$) and spin flip conductances ($g_{\uparrow\downarrow}$, $g_{\downarrow\uparrow}$) as a function of energy E for a diamond chain with 15 plaquettes when ϕ and tso are fixed to 0.4 and 4 , respectively. The parameters ϵ_A and ϵ_B are set to 0 .

energy characteristics are observed when we consider the effects of both the AB flux ϕ and Rashba SO coupling tso . The results are shown in Fig. 8 for a diamond chain with 15 identical diamond plaquettes when ϕ and tso are

fixed to 0.4 and 4 , respectively. For sufficiently high AB flux and Rashba strength two additional energy gaps occur at the flanks on both sides of the conductance spectrum in addition to the central gap. The energy gaps are positioned identically for all these spectra, but their magnitudes may differ.

It is important to note that when anyone of ϕ and tso is 0 and other is non-zero, $g_{\uparrow\uparrow}$ becomes exactly identical to $g_{\downarrow\downarrow}$, and so is $g_{\uparrow\downarrow}$ and $g_{\downarrow\uparrow}$. On the other hand, when both are non-zero, spin conserved conductances differ in magnitude, but the spin flip conductances remain identical. All these conductance-energy characteristics shown in Figs. 6-8 are compatible with the E - k diagrams presented in Fig. 3. The appearance of the gaps for the finite chain in each cases are in complete agreement with the dispersion curves obtained earlier for an infinite sized diamond chain.

D. DOS-energy characteristics

To justify the nature of energy eigenstates of such a quantum network now we address the behavior of average density of states. It is expressed as,

$$\rho_{av}(E) = -\frac{1}{\pi N} \text{Im}[\text{Tr}[\mathbf{G}]] \quad (31)$$

where, N being the total number of atomic sites in the diamond chain.

As illustrative examples in Fig. 9 we show the variations of average density of states as a function of energy E for a diamond chain considering 15 plaquettes with different parametric values of AB flux ϕ and Rashba SO coupling strength tso . In (a), ρ - E spectrum is given when both ϕ and tso are fixed at zero. The spectrum does not provide any gap throughout the spectrum which is expected. Additionally, a sharp localized state is observed at the band center i.e., at $E = 0$. This localized state

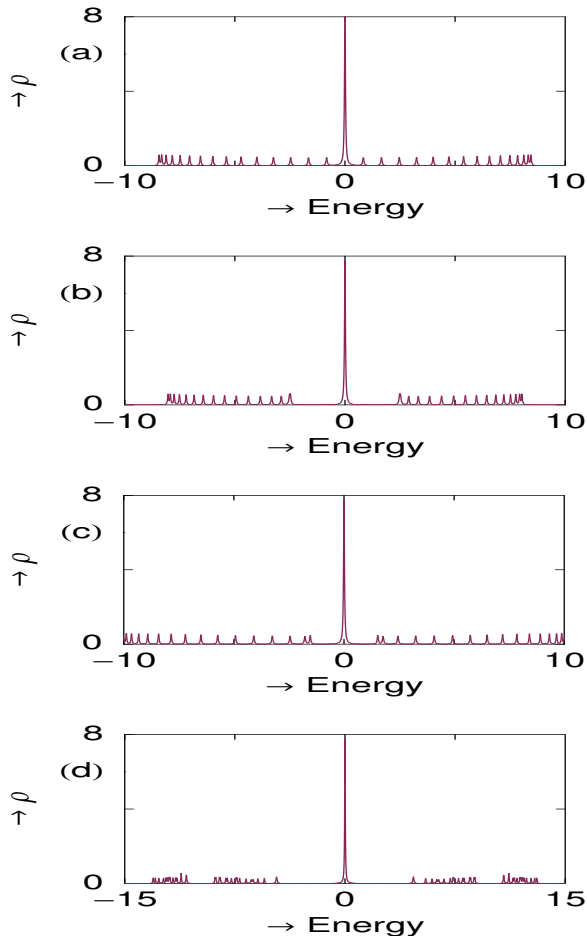


FIG. 9: (Color online). Average density of states as a function of energy E for a diamond chain considering 15 plaquettes with different values of ϕ and tso when $\epsilon_A = \epsilon_B = 0$. (a) $\phi = 0$, $tso = 0$; (b) $\phi = 0.2$, $tso = 0$; (c) $\phi = 0$, $tso = 2$ and (d) $\phi = 0.4$, $tso = 4$.

is highly degenerate and pinned at the typical energy $E = \epsilon_B$, and the existence of the localized state is the characteristic feature of such kind of quantum network as mentioned in the previous work [21]. In (b) and (c), an energy gap is visible at the center of the spectrum along with the presence of the sharp localized state at $E = 0$. By tuning the AB flux ϕ or Rashba coupling strength tso , the width of the gap can be controlled. Finally, in (d) the spectrum is shown when both ϕ and tso

are finite. In this particular case two extra gaps appear together with the central one at the two sides of the ρ - E spectrum. The localized state is also situated at the same place as earlier.

E. Effect of Rashba SO interaction on localization

In such a quantum network, AB flux can induce complete localization. At the typical flux $\phi = \phi_0/2$, conductance drops exactly to zero in the absence of Rashba SO interaction. This is due to the complete destructive inter-

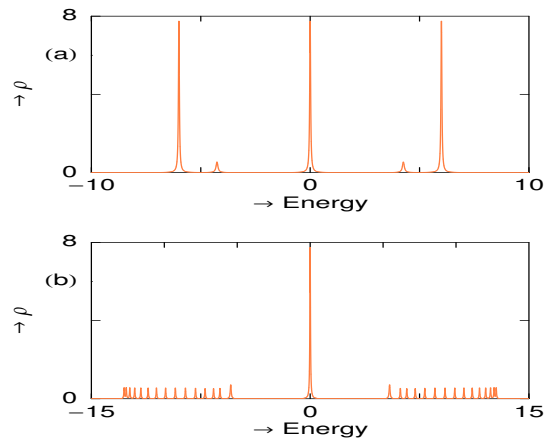


FIG. 10: (Color online). Average density of states as a function of energy for a diamond network considering 15 plaquettes with $\epsilon_A = \epsilon_B = 0$ when AB flux ϕ is set at $\phi_0/2$. (a) $tso = 0$ and (b) $tso = 2$.

ference among the electronic waves passing through different arms of the network. At $\phi = \phi_0/2$, two more localized states appear in the ρ - E characteristics (Fig. 10(a)) in addition to the previous one pinned at $E = 0$. The positions of these states can be evaluated exactly and they are expressed mathematically as,

$$E = \frac{1}{2} \left[(\epsilon_A + \epsilon_B) \pm \sqrt{(\epsilon_A + \epsilon_B)^2 - 4(\epsilon_A \epsilon_B - 4t^2)} \right] \quad (32)$$

In the presence of Rashba spin orbit interaction, the interference is not completely destructive anymore at $\phi = \phi_0/2$. The two additional localized states placed at the two opposite sides of the central localized state disappear for non-zero Rashba strength as clearly seen from Fig. 10(b). Rashba spin-orbit coupling affects the spin dynamics significantly resulting in a non-zero conductance at $\phi = \phi_0/2$.

F. Rashba induced semi-conducting behavior

Here we address how such a quantum network can be utilized to show semi-conducting behavior induced by Rashba SO interaction in the absence of any AB flux ϕ .

A similar type of semi-conducting nature controlled by AB flux has been established in such a system, where SO interaction was not considered [21]. To justify our idea, in Fig. 11 we plot the average density of states as a func-

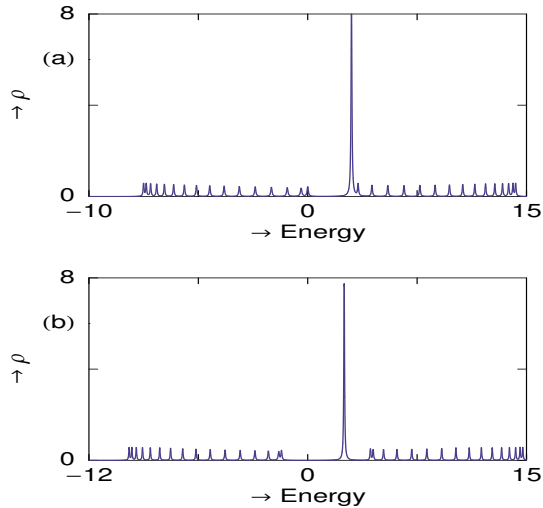


FIG. 11: (Color online). Average density of states as a function of energy for a diamond chain considering 15 plaquettes in the absence of AB flux ϕ where ϵ_A and ϵ_B are fixed at 0 and 2, respectively. (a) $tso = 0$ and (b) $tso = 2$.

tion of energy considering 15 plaquettes where ϵ_A and ϵ_B are set at 0 and 2, respectively. An energy gap automatically appears in the spectrum even when both ϕ and tso are identical to zero since we choose different values of ϵ_A and ϵ_B (see Fig. 11(a)) and a highly degenerate localized state is situated at the edge of the gap i.e., at $E = 2$. By controlling the external gate potential i.e., tuning the Rashba strength to a non-zero value the width of the gap can be increased arbitrarily as shown in Fig. 11(b), keeping the position of the localized state invariant. Now, if the Fermi level E_F is fixed at the energy $E = 2$ i.e., where the localized state is placed (see Fig. 11(b)) then for small Rashba coupling strength the gap between the localized level and the bottom of the right sub-band is small enough for the electrons to bridge. Therefore, the system behaves as a n -type semiconductor. Similarly, if ϵ_B is fixed at -2 and the Fermi level is set at the top of the left sub-band then the system can be implemented equivalently as a p -type semiconductor. In this case holes are created in the left sub-band. It is important to mention that when the site energies (ϵ_A and ϵ_B) are fixed at the same values then the system can also be used as a semi-conductor depending on the electron concentration. The detailed analysis is available in Ref. [21].

G. Spin filtering action

With proper tuning of the external parameters i.e., magnetic flux ϕ and Rashba strength tso such a network

can achieve a high degree of spin polarization as discussed earlier in a theoretical work by Aharony *et al.* [20]. Here, we discuss this feature from a different point of view.

When there is no external magnetic field or magnetic flux, time reversal symmetry is not broken i.e., the Hamiltonian of the system remains invariant under time reversal operation. Mathematically it is expressed as $[H_{SO}, T] = 0$, where T is the time reversal operator. The Rashba Hamiltonian (H_{SO}) is usually written as,

$$\begin{aligned} H_{SO} &= \frac{\alpha_R}{\hbar} (\vec{\sigma} \times \vec{p})_z \\ &= i\alpha_R \left(\sigma_y \frac{\partial}{\partial x} - \sigma_x \frac{\partial}{\partial y} \right) \end{aligned} \quad (33)$$

and $T = i\sigma_y \hat{C}$, \hat{C} being the complex conjugation operator. The second quantized form of Eq. (33) is given by the fourth and fifth terms of Eq. (2). As electrons are spin- $\frac{1}{2}$ particles, so following Kramer's theorem, each

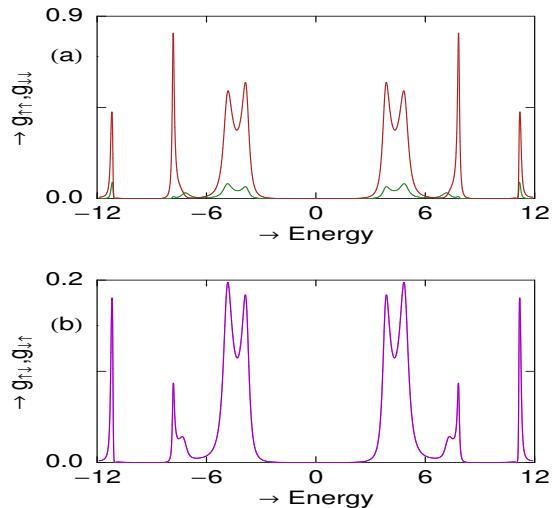


FIG. 12: (Color online). Variation of conductances as a function of energy for a diamond chain with 3 plaquettes considering $\phi = 0.3$ and $tso = 4$ where $\epsilon_A = \epsilon_B = 0$. In (a) $g_{\uparrow\uparrow}$ and $g_{\downarrow\downarrow}$ and in (b) $g_{\uparrow\downarrow}$ and $g_{\downarrow\uparrow}$ are superposed to each other.

eigenstate is at least two-fold degenerate and spin is no longer a good quantum number in the presence of spin-orbit interaction. *In many cases the degeneracy implied by Kramer's theorem is merely the degeneracy between states of spin up and spin down, or something equally obvious. The theorem is non-trivial for a system with spin-orbit coupling in an unsymmetrical electric field, so that neither nor angular momentum is conserved. Kramer's theorem implies that no such field can split the degenerate pairs of energy levels* [23].

However, the degeneracy can be removed by applying external magnetic flux or magnetic field as in this case time reversal symmetry is not conserved anymore and therefore spin polarization can be achieved. The degree of polarization of the transmitted electrons is convention-

ally defined as,

$$P(E) = \left| \frac{(g_{\uparrow\uparrow} + g_{\downarrow\uparrow}) - (g_{\downarrow\downarrow} + g_{\uparrow\downarrow})}{(g_{\uparrow\uparrow} + g_{\downarrow\uparrow}) + (g_{\downarrow\downarrow} + g_{\uparrow\downarrow})} \right| \quad (34)$$

For our illustrative purpose, in Fig. 12 we plot the variations of conductances as a function of energy for a diamond network with three plaquettes considering $\phi = 0.3$ and $tso = 4$. A significant change is observed in the magnitudes of spin conserved conductances ($g_{\uparrow\uparrow}$ and $g_{\downarrow\downarrow}$) (Fig. 12(a)), while the spin flip conductances ($g_{\uparrow\downarrow}$ and $g_{\downarrow\uparrow}$) are identical as shown in Fig. 12(b). Therefore, applying a non-zero flux spin polarization is clearly obtained. Following Eq. (34) we calculate the degree of polarization for an arbitrary energy $E = -5$ (say), and it shows 44%.

IV. CLOSING REMARKS

To conclude, in the present work we have explored spin dependent transport through an array of diamonds where each diamond plaquette is threaded by an AB flux ϕ considering the effect of Rashba SO interaction. The diamond chain is directly coupled to two semi-infinite 1D non-magnetic metallic leads, namely, source and drain. We have adopted a discrete lattice model in the tight-

binding framework to describe the system and all the results have been obtained by using Green's function formalism. With a detailed analytical description of energy dispersion relation for an infinite diamond network considering the effect of Rashba SO interaction, we have presented the numerical results of the conductance-energy characteristics in addition to the average density of states of a finite sized diamond array to establish the idea for a realistic system. We have also studied the delocalizing effect for the network in the presence of Rashba SO interaction when the AB flux ϕ is set at $\phi_0/2$. Finally, we have shown that depending on the specific choices of SO interaction strength and AB flux, the quantum network can be utilized as a spin filter.

In the present work we have calculated all these results by ignoring the effects of temperature, electron-electron correlation, electron-phonon interaction, disorder, etc. Here, we set the temperature at 0K, but the basic features will not change significantly even in non-zero finite (low) temperature region as long as thermal energy ($k_B T$) is less than the average energy spacing of the energy levels of the diamond chain. In this model it is also assumed that the two side-attached non-magnetic leads have negligible resistance. Our presented results may be useful in designing spin based nano electronic devices.

-
- [1] S. A. Wolf, D. D. Awschalom, R. A. Buhrman, J. M. Daughton, S. von Molnar, M. L. Roukes, A. Y. Chtchelkanova, and D. M. Treger, *Science* **294**, 1488 (2001).
 - [2] M. N. Baibich, J. M. Broto, A. Fert, F. N. Van Dau, F. Petroff, P. Etienne, G. Creuzet, A. Friederich, and J. Chazelas, *Phys. Rev. Lett.* **61**, 2472 (1998).
 - [3] W. Long, Q. F. Sun, H. Guo, and J. Wang, *Appl. Phys. Lett.* **83**, 1397 (2003).
 - [4] P. Zhang, Q. K. Xue, and X. C. Xie, *Phys. Rev. Lett.* **91**, 196602 (2003).
 - [5] Q. F. Sun and X. C. Xie, *Phys. Rev. B* **91**, 235301 (2006).
 - [6] Q. F. Sun and X. C. Xie, *Phys. Rev. B* **71**, 155321 (2005).
 - [7] F. Chi, J. Zheng, and L. L. Sun, *Appl. Phys. Lett.* **92**, 172104 (2008).
 - [8] T. P. Pareek, *Phys. Rev. Lett.* **92**, 076601 (2004).
 - [9] W. J. Gong, Y. S. Zheng, and T. Q. Lü, *Appl. Phys. Lett.* **92**, 042104 (2008).
 - [10] H. F. Lü and Y. Guo, *Appl. Phys. Lett.* **91**, 092128 (2007).
 - [11] Y. A. Bychkov and E. I. Rashba, *Sov. Phys. JETP* **39**, 78 (1984).
 - [12] T. P. Pareek and P. Bruno, *Phys. Rev. B* **65**, 241305(R) (2002).
 - [13] F. Mireles and G. Kirczenow, *Phys. Rev. B* **64**, 024426 (2001).
 - [14] N. Hatano, R. Shirasaki, and H. Nakamura, *Phys. Rev. B* **75**, 032107 (2007).
 - [15] G. Lommer, F. Malcher, and U. Rossler, *Phys. Rev. Lett.* **60**, 728 (1988).
 - [16] J. Nitta, T. Akazaki, H. Takayanagi, and T. Enoki, *Phys. Rev. Lett.* **78**, 1335 (1997).
 - [17] C. Hu, J. Nitta, T. Akazaki, H. Takayanagi, J. Osaka, P. Pfeffer, and W. Zawadzki, *Phys. Rev. B* **60**, 7736 (1999).
 - [18] M. I. D'yakonov and V. I. Perel', *Sov. Phys. JETP* **33**, 1053 (1971).
 - [19] D. Bercioux, M. Governale, V. Cataudella, and V. M. Ramaglia, *Phys. Rev. B* **72**, 075305 (2005).
 - [20] A. Aharony, O. E. -Wohlman, Y. Tokura, and S. Katsumoto, *Phys. Rev. B* **78**, 125328 (2008).
 - [21] S. Sil, S. K. Maiti, and A. Chakrabarti, *Phys. Rev. B* **79**, 193309 (2009).
 - [22] S. Datta, *Quantum Transport: Atom to Transistor*, Cambridge University Press, Cambridge (2005).
 - [23] L. E. Ballentine, *Quantum Mechanics: A Modern Development*, World Scientific Publishing, (1998).